

Role of tantalum concentration on the high dose self-ion irradiation behavior of nanocrystalline binary alloys

S. Srinivasan ^a, B.C. Hornbuckle ^b, M. Chancey ^c, K.A. Darling ^b, Y.Q. Wang ^c, K. Solanki ^{a,*}

^a School for the Engineering of Matter, Transport, and Energy, Arizona State University, Tempe, AZ 85287, USA

^b DEVCOM Army Research Laboratory, Weapons and Materials Research Directorate, APG, MD 21014, USA

^c Materials Science and Technology Division, Los Alamos National Laboratory, Los Alamos, NM 87545, USA

ARTICLE INFO

Keywords:

Nanocrystalline
Irradiation
Grain growth
Kinetic stability

ABSTRACT

In this work, the self-ion irradiation behavior of nanocrystalline copper-tantalum alloys was investigated. In particular, the microstructural evolution of Cu-3at.%Ta and Cu-10at.%Ta was evaluated under the fluence of 2×10^{17} ions/cm² of 4 MeV Cu-ions at different temperatures. Results revealed that despite the ability of Cu-10Ta to reprecipitate new nanoclusters and thereby increase the sink density by ~17%, it undergoes significant microstructural evolution. On the other hand, Cu-3Ta exhibits a relatively more stable microstructural response and 3.5 times less swelling over the same conditions. This result illustrates the premise that irradiation and deformation may be coupled to stabilize/rejuvenate Ta-nanoclusters in extreme-environments.

Designing and developing materials that can withstand harsh nuclear environments is of great importance to ensure the safe and efficient performance of reactors [1]. While nanocrystalline (NC) materials, i.e. metals with mean grain size (d) below 100 nm, are known to be a promising candidate for radiation-tolerant structures owing to their high density of interfaces that can neutralize radiation-induced defects [2,3], their microstructural instability to stimuli such as temperature, stress, and intense radiation has greatly limited their ability to operate under the long-term environments required for nuclear power reactors [4]. Through years of computational research and eventual experimental efforts, grain boundary (GB) stabilization has become viable through solute addition that either lowers the GB excess free energy (thermodynamic stabilization) or forms atomic clusters that pin the GB, thereby restraining the GB mobility (kinetic stabilization) [5,6]. In addition to GBs, immiscible metal alloys introduce numerous sharp interfaces between the phases due to their phase-separating nature [7].

In such materials with high sink density, irradiation-induced point defects primarily interact with and potentially accumulate at the interfaces (GBs and phase boundaries). Such defect accumulation can affect the structural stability of interfaces causing grain growth [8], dissolution, disordering, or coarsening of second phase particles [9], depending on the nature and sink efficiency of the interface [10]. As mentioned before, since the concern with grain growth in nanocrystalline materials can be addressed by appropriate solute additions that segregate to and pin the GB, the overall behavior of such a system

depends on the behavior and stability of the second phase particles. Mechanisms of phase stability (e.g., forced atomic mixing, ballistic dissolution, Ostwald-ripening, inverse Ostwald-ripening, etc.) in systems driven far from equilibrium either through processing or through high energy irradiation have been vastly discussed theoretically and experimentally in various alloys [11–14].

Previous works on NC-Cu-10at.%Ta (Cu-10Ta) have shown exceptional thermomechanical properties [15–17], microstructural stability, and self-healing of radiation damage through the re-precipitation of Ta clusters [18,19]. In addition, this alloy can provide thermal conductivity 5–10 times higher than currently-used materials [17,20]. Therefore, provides opportunities for developing next-generation high-temperature (HT), high-pressure (HP), high-performance heat exchangers (H3HX) in pressurized water reactors (PWR), gas turbines, and hot gas heat recovery applications. Though the response of second phase particles and their role in stabilizing and increasing the sink density have been shown in previous studies [18,19,21], the effect of solute concentration on the precipitate type and/or formation has not been closely examined. Such an understanding, combined with the aforementioned understanding of particles and sink density, would enable the ability to tailor the composition and/or microstructure for improved phase stability and radiation resistance. Thus, in this work, we compare the high-dose self-ion irradiation response of Cu-3at.%Ta (Cu-3Ta) and Cu-10Ta to understand the role of tantalum concentration in suppressing the effect of atomic mixing at extreme doses and enhancing radiation tolerance.

* Corresponding author.

E-mail address: kiran.solanki@asu.edu (K. Solanki).

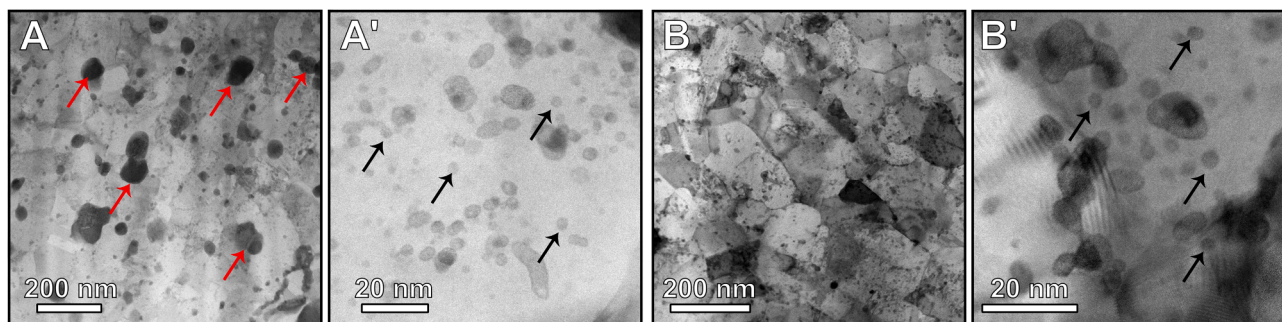


Fig. 1. Aberration Corrected (AC) bright field STEM images of the As-received microstructure. Images (A-A') NC-Cu-10Ta and (B-B') NC-Cu-3Ta depict the difference in density of large Ta-particles between 10% and 3%. (Red arrows indicated Large Ta particles and Black arrows the Ta-based nanoclusters)

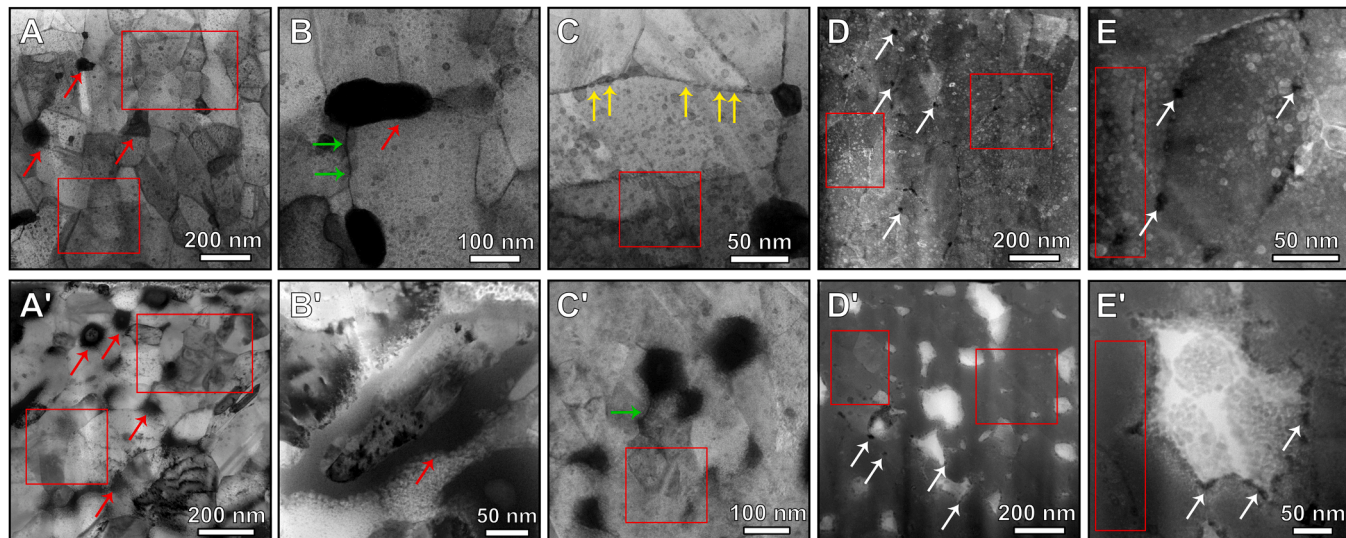


Fig. 2. AC bright field STEM images of the Post irradiation microstructure at RT of Cu-3at.%Ta and Cu-10at.%Ta. Microstructure irradiated to 100 dpa at RT of (A-E) NC Cu-3Ta alloy showing stable grains and nanoclusters and voids along some GBs (A'-E') Cu-10Ta. (Red arrows point to the interface of the large Ta-particles; Green arrows Ta solute along GBs; Yellow arrows Ta-nanoclusters precipitated along GBs; White arrows voids and void channels; and Red boxes highlight the difference in nanocluster density).

NC Cu-3Ta was chosen for the study from several compositions to have a tailored microstructure with minimum large incoherent precipitates without significantly compromising on grain size and nanocluster density [22]. The similarity in grain size and nanocluster density should enable an understanding as to the role of Ta precipitates on improved radiation tolerance in this alloy system.

Toward this, NC Cu-3Ta and Cu-10Ta were produced by high-energy mechanical alloying and consolidated by equal channel angular extrusion (ECAE) [23,24]. The consolidated ingots were machined into cylindrical specimens having 3 mm diameter and ~1.2 mm tall. These samples were mechanically polished to a mirror finish and subsequently irradiated with 4 MeV Cu⁺⁺ ions in a defused beam mode using a 3 MV Pelletron tandem ion accelerator at Ion Beam Materials Laboratory at Los Alamos National Laboratory. A flux of $\sim 9 \times 10^{12}$ ions $\text{cm}^{-2} \text{s}^{-1}$ was used to achieve a fluence of 2×10^{17} ions cm^{-2} at room temperature (RT) and 573 K. Damage profiles in displacements per atom (dpa, Appendix Fig. A1), indicate a damage level of 100 dpa near the surface, with peak damage of ~ 300 dpa occurring at $\sim 1 \mu\text{m}$. For pre- and post-irradiated microstructural characterization, transmission electron microscopy (TEM) characterization was conducted using an ARM-200F. TEM samples were generated using a Focused Ion beam (FIB) FEI Nova 500 allowing the lifted-out specimen to contain the irradiated regions of interest. Once lifted out, the specimen was thinned to electron transparency with the final step conducted at 2 keV; additionally, they were plasma cleaned in Ar before TEM observations to reduce contamination. Grain size statistics were obtained from the irradiated samples analyzing

grains with depths ranging from 100-600 nm from the top surface; this statistical analysis utilized the ImageJ software. Atom probe tomography (APT) specimens were prepared using a ThermoFisher Scientific Helios G4 dual-beam microscope with final annular milling occurring at 5keV. APT was performed using a Cameca LEAP 5000 XR system operated at 50 K with laser energy of 50 pJ, auto pulse rate control enabled with a minimum mass spectrum range of 300 Da, and a target evaporation rate of 0.5%. The analysis was performed using IVAS 3.8.4 software. The envelop method was utilized for the cluster analysis with a maximum separation distance of 0.75 nm (d_{\max}); a group of TaO ions composed of at least 15 ions (N_{\min}) was identified as a cluster. The total number of clusters analyzed for each condition of Cu-3Ta was greater than 750, similar to that for the Cu-10Ta.

As received microstructure of Cu-3Ta and Cu-10Ta are shown in Fig. 1, which depicts the key differences in their microstructure. Cu-10Ta exhibits an NC copper grain size on the order of 50 nm, while Cu-3Ta has a slightly larger grain size of 99 nm [25]. For the tantalum phase, Cu-10Ta has a bimodal size distribution with the presence of large incoherent Ta precipitates (being > 30 nm on average) and smaller nanoclusters (~ 3 nm on average) shown in red and black arrows respectively (Fig. 1A-A'). Prior work by the authors has determined that Ta-based precipitates have coherent, semi-coherent, and incoherent nanoclusters when the diameter (d) of the precipitate is: < 3.9 nm, 3.9 to 15.6 nm, and > 15.6 nm, respectively [26]. In contrast, Cu-3Ta possesses primarily just nanoclusters with a very limited concentration of these larger incoherent Ta precipitates (Fig. 1B-B'). Previous APT studies have

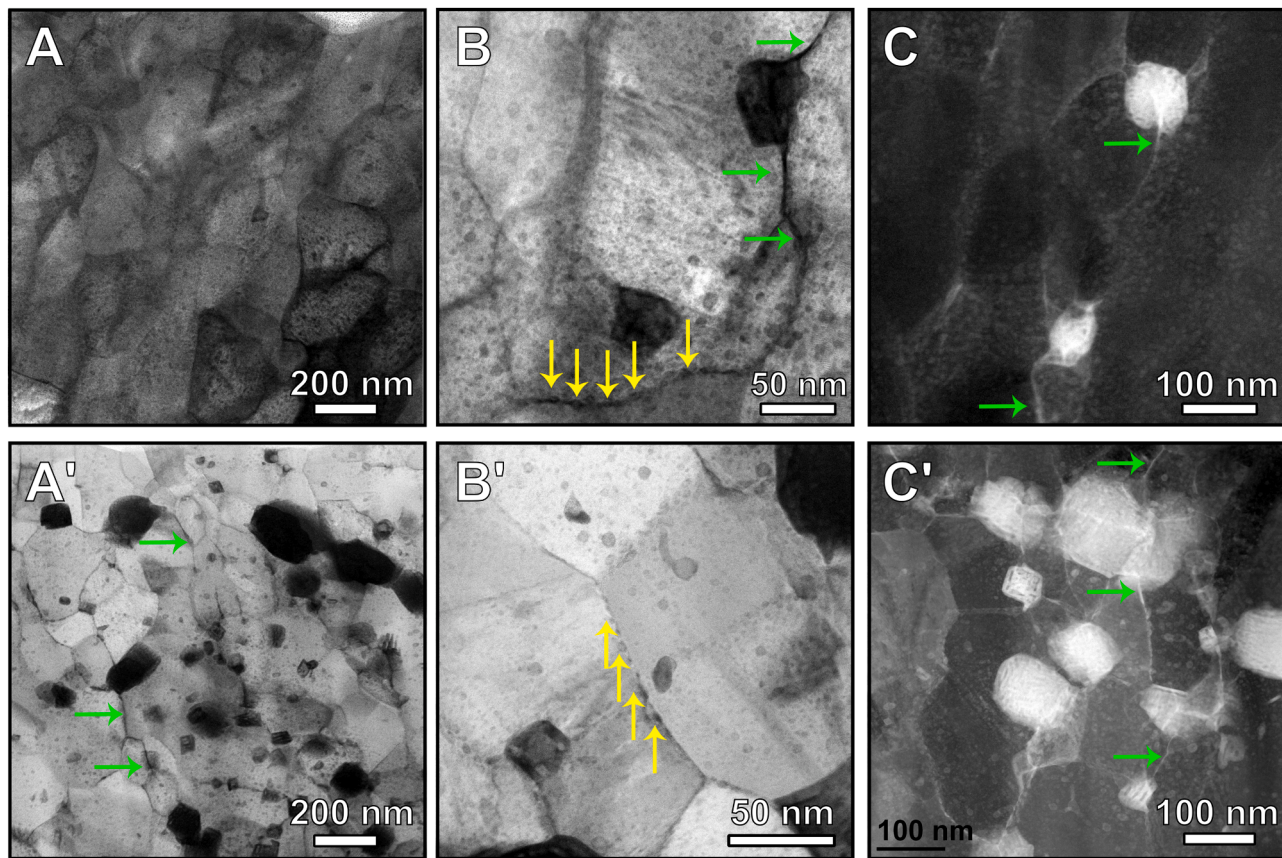


Fig. 3. AC bright field and high angular annular dark-field STEM images of the Post irradiation microstructure at 573 K of Cu-3at.%Ta and Cu-10at.%Ta. A-B and A'-B' are bright field images. C and C' are high angular annular dark field images. Microstructure irradiated to 100 dpa at 573 K of (A-C) NC Cu-3Ta alloy showing stable grains and nanoclusters and voids along some GBs (A'-C') Cu-10Ta. Green arrows point to Ta solute along GBs; Yellow arrows Ta nanoclusters precipitated along GBs

indicated a nanocluster density of $6.5 \times 10^{23} / \text{m}^3$ and $5.4 \times 10^{23} / \text{m}^3$ (18% less) in Cu-10Ta and Cu-3Ta, respectively, for the samples after ECAE processing at 973 K [22,23]. In our previous work, Cu-10Ta was able to demonstrate an increased radiation immunity as well as self-healing from radiation damage through the re-precipitation of Ta clusters [18]. This effect was attributed to larger Ta-particles undergoing ballistic dissolution followed by re-precipitation as nanoclusters, thereby replenishing the sink strength. This behavior, in turn, served to enhance the radiation tolerance of the material when exposed to high irradiation doses and elevated temperatures. Given the large disparity in these larger Ta particles between the Cu-10Ta and Cu-3Ta alloys, one would expect to see a difference in the comparative response/stability of these two alloy types when irradiated under identical conditions.

To compare the microstructural and phase stability at high doses, the specimens were first irradiated at room temperature to 100 dpa. Fig. 2 presents the grain size in both alloys. Post-irradiation analysis for Cu-10Ta found that the average grain size had increased by ~ 60 nm. Cu-3Ta alloy underwent an equal amount of grain growth yielding an average grain size of ~ 160 nm. Looking at the phase stability, the high dose rate in heavy-ion at RT, resulted in the disordering of the large incoherent Ta-precipitate interfaces in Cu-10Ta (see Fig. 2A'-B' and Appendix Fig. A2). Furthermore, a significant reduction in Ta-cluster density was observed in many grains indicating the ballistic dissolution of the nanoclusters in the regions undergoing an amorphous transformation. This effect inherently lowers the overall cluster density within the alloy. However, unlike the Cu-10Ta sample, TEM images of Cu-3Ta indicated much higher retention of Ta clusters, as seen in Fig. 2 where the red boxes highlight the comparative difference between the two alloys in this respect. Interestingly, the few larger Ta particles found to exist in Cu-3Ta did not inherently undergo an amorphous

transformation (Fig. 2B). For both cases, several GBs were found to be saturated in Ta solute near the dissolution of these larger Ta particles (see green arrows in Fig. 2).

Additionally, sporadic void formation was also observed in both these alloys after some incubation time (see also Fig. 2 white arrow). Specifically, in Cu-10Ta, voids of an average size of ~ 12 nm were mainly observed to be formed along the large tantalum interfaces which showed initial transient disordering, followed by dissolution. As indicated in Fig. 2, some of these incoherent interfaces also had void channels resulting from the coalescence of these voids (Fig. 2E-E'). The maximum swelling observed was $\sim 0.25\%$. On the other hand, in Cu-3Ta, the voids were smaller, on the order of ~ 7 nm, and comparatively lesser in density than Cu-10Ta. The voids in Cu-3Ta were mostly confined to the GBs (Fig. 2E) with a maximum swelling of 0.07%. Moreover, unlike the incoherent disordered interfaces in Cu-10Ta, the presence of nanoclusters at GBs in Cu-3Ta also suppressed the channeling of these voids in these regions (Fig. 2 yellow arrows).

At 573 K, no voids or amorphization were observed in both Cu-10Ta and Cu-3Ta samples. At this temperature, however, Cu-10Ta showed a significant increase in cluster density. This is likely due to nanocluster re-precipitation from within the regions near the dissolved larger Ta precipitates. This is attributed to the high positive enthalpy of mixing of Ta in Cu [27]. Similar ballistic dissolution and short circuit diffusion of Ta from large Ta-precipitates along the GBs were observed in Cu-3Ta with high cluster density around these regions (Fig. 3 B-C green and yellow arrows), indicating similar re-precipitation. This is possible given the intense amount of radiation-induced defects and their thermally induced annihilation, which could act to promote the decomposition of Ta-saturated regions of solute within the lattice [18]. As can be observed in the high-angle annular dark field (HAADF) images of Fig. 3, diffusion

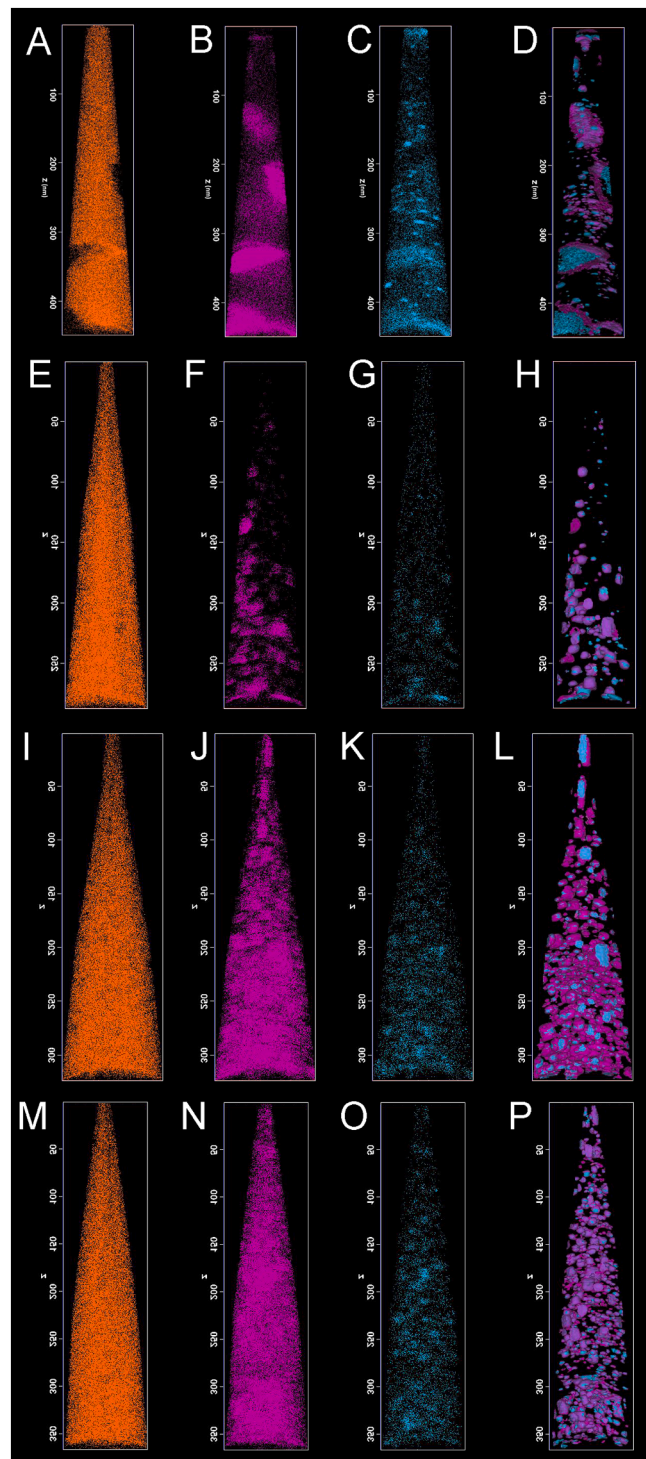


Fig. 4. Atom probe reconstruction for Cu-3Ta and Cu-10Ta at 100 dpa at RT and 573 K. Atom probe distribution of Cu (A, E, I, and M), Ta (B, F, J, and N), O (C, G, K, and O), and only the 5.5 at.% TaO isoconcentration surfaces (D, H, L, and P) are displayed to highlight the number density of said particles within the tip. Images A-D are for Cu-10Ta at RT, images E-H are for Cu-10Ta at 573 K, images I-L are for Cu-3Ta at RT, and images M-P are for Cu-3Ta at 573 K.

of Ta solute along GBs (green arrow) is observed for both 3 and 10 at% Ta. This was found to be more prevalent and extensive than that occurred following room temperature irradiation.

Though the microstructure of the Cu-10Ta alloy can self-heal through the generation of new nanoclusters and reordering of interfaces at 573 K, it is clear through the TEM analysis that its

microstructure is somewhat unstable at RT. In contrast, Cu-3Ta shows a nearly unaffected cluster density throughout the same conditions while at the same time retaining its nanocrystalline microstructure. APT was utilized to characterize the number density of the Ta-based clusters for the RT and 573 K conditions for both alloys. Fig. 4 provides the APT reconstruction for all four samples. Interestingly, it was determined that the number density is approximately the same, that is for Cu-10Ta, the cluster density was found to be $7.6 \times 10^{23} / \text{m}^3$ and that of Cu-3Ta was $8.8 \times 10^{23} / \text{m}^3$ after irradiated at 573 K. Both alloys post-irradiation have higher cluster densities than prior to exposure (the respective as-received cluster densities were $5.4 \times 10^{23} / \text{m}^3$ for Cu-3Ta and $6.5 \times 10^{23} / \text{m}^3$ for Cu-10Ta, respectively). These numbers are for qualitative comparison as the two alloys have similar cluster densities. However, the Cu-3Ta alloy is much more stable with respect to undergoing drastic phase transformations and/or large changes in the number density of Ta-based clusters through the process. That is, despite the ability of Cu-10Ta to reprecipitate new clusters, it underwent significant microstructural evolution as compared to Cu-3Ta. Conversely, Cu-3Ta exhibited a relatively stable, more predictable response over the same conditions. More recently, Cu-3Ta was also shown to be the most microstructurally resistant to change under prolonged high-temperature exposure (1,000 h at 80% T_m of copper, i.e., 1073 K) relative to other higher or lower Ta concentrations [28]. The same may hold true regarding radiation-induced coarsening. In other words, while both alloys display a high degree of microstructural stability, Cu-3Ta distinguishes itself as the composition with a greater degree of microstructural stability to applied stimuli. In other words, the limited density of large precipitates and more clusters replacing them act as efficient defect sinks thereby preventing/increasing the threshold of such defect accumulation in the large tantalum precipitates and GBs in Cu-3Ta.

In summary, the phase stability and its effect on radiation tolerance of two different compositions of Cu-Ta system (3 at.% Ta and 10 at.% Ta) are studied using high dose, heavy ion irradiation at RT and 573 K. The results indicate that Cu-3Ta shows more promise when exposed to high dose radiation and better resistance to radiation-induced atomic mixing than Cu-10Ta owing to the near absence of the incoherent large Ta-precipitates. Furthermore, the void swelling observed was 3.5x less than that of Cu-10Ta indicating the presence of potentially higher semi-coherent cluster density which needs to be confirmed comprehensively with additional experiments.

Declaration of Competing Interest

The authors declare that they have no known competing financial interests or personal relationships that could have appeared to influence the work reported in this paper.

Acknowledgment

S.S. and K. S. acknowledge the use of facilities within the LeRoy Eyring Center for Solid State Science at Arizona State University. This work was supported by the US Army Research Laboratory under contract W911NF-15-2-0038 and the National Science Foundation under grants No. 1663287 and 1810431. This work was performed, in part, at the Center for Integrated Nanotechnologies, an Office of Science User Facility operated by the U.S. Department of Energy (DOE) Office of Science. Los Alamos National Laboratory, an affirmative action-equal opportunity employer, is managed by Triad National Security, LLC for the U.S. Department of Energy's NNSA, under contract 89233218CNA000001.

Appendix

Figs. A1–A3

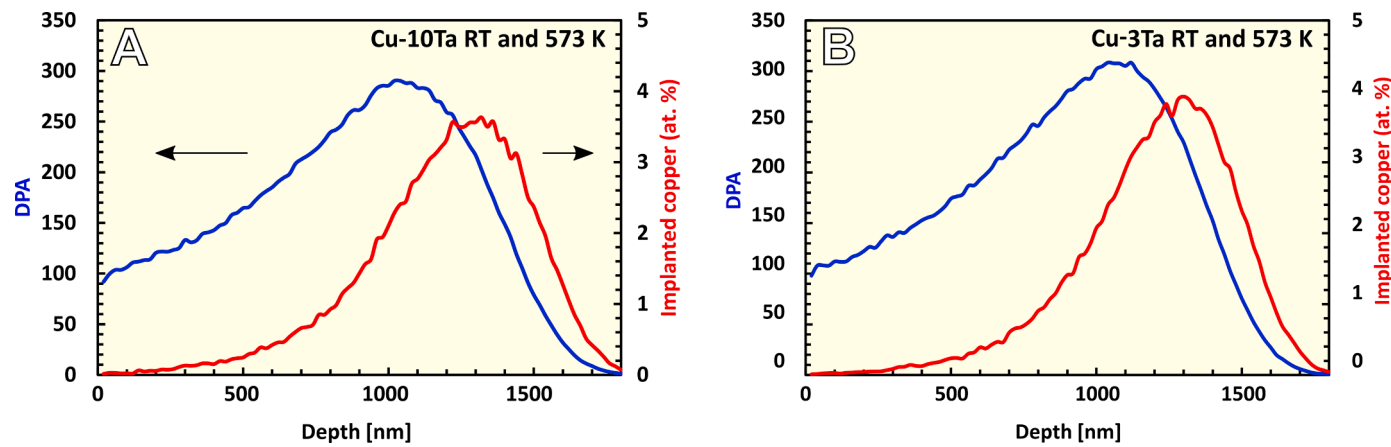


Fig. A1. SRIM Damage profile. Dpa profile and range for NC Cu-10Ta and Cu-3Ta alloys irradiated with 4 MeV Cu⁺⁺ ions at room temperature and 573 K.

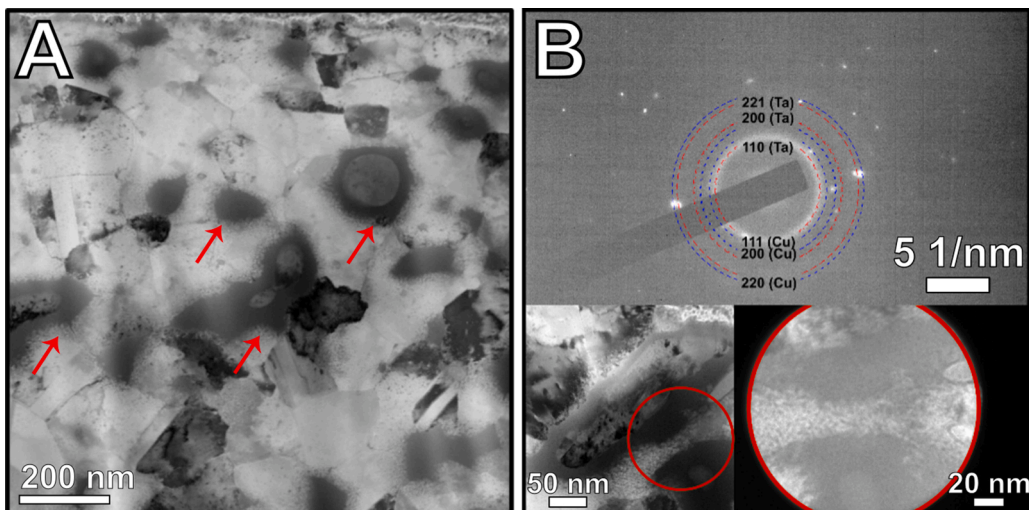


Fig. A2. AC bright field STEM images of the post irradiation microstructure at RT of Cu-10at.%Ta. (A) General microstructure where red arrows point to the interface between the matrix and the large disordered Ta particles. (B) The diffraction pattern is taken from within the red circle, indicating a disordered structure, along with higher magnification images of the Ta/Cu interface.

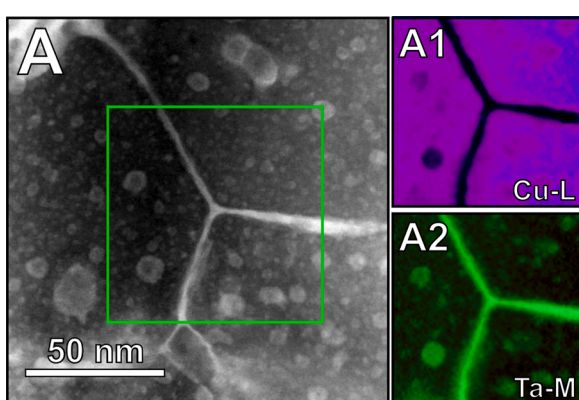


Fig. A3. Elemental analysis of Ta segregation under high self-ion irradiation at a higher temperature. (A) HAADF image showing a dissolving Ta particle preferentially diffusing along a GB. (A1) EELS Cu-L map in purple, of the region highlighted by the green box in A, showing the GB region devoid of copper. (A2) Ta-M map in green, of the same region.

References

- [1] G.S. Was, D. Petti, S. Ukai, S. Zinkle, J. Nucl. Mater. 527 (2019) 151837.
- [2] S. Wurster, R. Pippan, Scr. Mater. 60 (2009) 1083–1087.
- [3] Y.-Q. Chang, Q. Guo, J. Zhang, L. Chen, Y. Long, F.-R. Wan, Front. Mater. Sci. 7 (2013) 143–155.
- [4] M. Jin, P. Cao, M.P. Short, Scr. Mater. 163 (2019) 66–70.
- [5] C.C. Koch, R.O. Scattergood, M. Saber, H. Kotan, J. Mater. Res. 28 (2013) 1785–1791.
- [6] C.C. Koch, R.O. Scattergood, K.A. Darling, J.E. Semones, J. Mater. Sci. 43 (2008) 7264–7272.
- [7] R.K. Koju, K.A. Darling, L.J. Kecske, Y. Mishin, JOM 68 (2016) 1596–1604.
- [8] D. Kaoumi, A.T. Motta, R.C. Birtcher, J. Appl. Phys. 104 (2008), 073525.
- [9] J.P. Wharry, M.J. Swenson, K.H. Yano, J. Nucl. Mater. 486 (2017) 11–20.
- [10] W.Z. Han, M.J. Demkowicz, E.G. Fu, Y.Q. Wang, A. Misra, Acta Mater. 60 (2012) 6341–6351.
- [11] K.C. Russell, Prog. Mater. Sci. (n.d.) 206.
- [12] K.C. Russell, J. Nucl. Mater. 206 (1993) 129–138.
- [13] R.S. Nelson, J.A. Hudson, D.J. Mazey, J. Nucl. Mater. 44 (1972) 318–330.
- [14] P. Wilkes, J. Nucl. Mater. 83 (1979) 166–175.
- [15] K.A. Darling, M. Rajagopalan, M. Komarasamy, M.A. Bhatia, B.C. Hornbuckle, R. S. Mishra, K.N. Solanki, Nature 537 (2016) 378–381.
- [16] S.A. Turnage, M. Rajagopalan, K.A. Darling, P. Garg, C. Kale, B.G. Bazehhour, I. Adlakha, B.C. Hornbuckle, C.L. Williams, P. Peralta, K.N. Solanki, Nat. Commun. 9 (2018) 2699.
- [17] M. Rajagopalan, K.A. Darling, C. Kale, S.A. Turnage, R.K. Koju, B.C. Hornbuckle, Y. Mishin, K.N. Solanki, Mater. Today 31 (2019) 10–20.
- [18] S. Srinivasan, C. Kale, B.C. Hornbuckle, K.A. Darling, M.R. Chancey, E. Hernández-Rivera, Y. Chen, T.R. Koenig, Y.Q. Wang, G.B. Thompson, K.N. Solanki, Acta Mater. 195 (2020) 621–630.

- [19] S. Srinivasan, B.C. Hornbuckle, K.A. Darling, H. Kim, Y.Q. Wang, K. Solanki, *Scr. Mater.* 208 (2022), 114344.
- [20] H.S. Lee, *Thermal Design: Heat Sinks, Thermoelectrics, Heat Pipes, Compact Heat Exchangers, and Solar Cells*, John Wiley & Sons, 2010.
- [21] P.V. Patki, Y. Wu, J.P. Wharry, *Materialia* 9 (2020), 100597.
- [22] B.C. Hornbuckle, K. Solanki, K.A. Darling, *Mater. Sci. Eng. A* 824 (2021), 141818.
- [23] B.C. Hornbuckle, T. Rojhirunsakool, M. Rajagopalan, T. Alam, G.P.P. Pun, R. Banerjee, K.N. Solanki, Y. Mishin, L.J. Kecske, K.A. Darling, *JOM* 67 (2015) 2802–2809.
- [24] V.H. Hammond, T.L. Luckenbaugh, M. Aniska, D.M. Gray, J.A. Smeltzer, B. C. Hornbuckle, C.J. Marvel, K.N. Solanki, T. Schmitz, K.A. Darling, *Adv. Eng. Mater.* 20 (2018), 1800405.
- [25] S. Srinivasan, S. Sharma, S. Turnage, B.C. Hornbuckle, C. Kale, K.A. Darling, K. Solanki, *Acta Mater.* 208 (2021), 116706.
- [26] M. Rajagopalan, K. Darling, S. Turnage, R. Kojju, B. Hornbuckle, Y. Mishin, K. Solanki, *Mater. Des.* 113 (2017) 178–185.
- [27] K.A. Darling, M.A. Tschopp, B.K. VanLeeuwen, M.A. Atwater, Z.K. Liu, *Comput. Mater. Sci.* 84 (2014) 255–266.
- [28] B.C. Hornbuckle, K.N. Solanki, K.A. Darling, *Mater. Sci. Eng. A* (2021).